HHS Public Access

Author manuscript

J Cell Physiol. Author manuscript; available in PMC 2019 December 01.

Published in final edited form as:

J Cell Physiol. 2018 December ; 233(12): 9548–9562. doi:10.1002/jcp.26858.

RUMI is a novel negative prognostic marker and therapeutic target in Non-Small Cell Lung Cancer

May Chammaa[*], **Agnes Malysa**[†], **Carlos Redondo**[*], **Hyejeong Jang**[‖], **Wei Chen**[†,‡,§,‖], **Gerold Bepler**[†,‡,#], and **Rodrigo Fernandez-Valdivia**[*,†,‡,§]

[*]Department of Pathology, Wayne State University School of Medicine, Detroit, MI 48201

[†]Department of Oncology, Wayne State University School of Medicine, Detroit, MI 48201

[‡]Cancer Biology Graduate Program, Wayne State University School of Medicine, Detroit, MI 48201

[§]Tumor Biology & Microenvironment Program, Wayne State University School of Medicine, Detroit, MI 48201

[‖]Biostatistics Core, Wayne State University School of Medicine, Detroit, MI 48201

[#]Molecular Therapeutics Program, Barbara Ann Karmanos Cancer Institute. Detroit, MI 48201

Abstract

Recent comprehensive next-generation genome and transcriptome analyses in lung cancer patients, several clinical observations, and compelling evidence from mouse models of lung cancer have uncovered a critical role for Notch signaling in the initiation and progression of Non-Small Cell Lung Cancer (NSCLC). Notably, Rumi is a "protein *O*-glucosyltransferase" that regulates Notch signaling through *O*-glucosylation of Notch receptors, and is the only enzymatic regulator whose activity is required for both ligand-dependent and ligand-independent activation of Notch. We have conducted a detailed study on RUMI's involvement in NSCLC development and progression, and have further explored the therapeutic potential of its targeting in NSCLC. We have determined that Rumi is highly expressed in the alveolar and bronchiolar epithelia, including Club cells and alveolar type II cells. Remarkably, *RUMI* maps to the region of chromosome 3q that corresponds to the major signature of neoplastic transformation in NSCLC, and is markedly amplified and overexpressed in NSCLC tumors. Notably, RUMI expression levels are predictive of poor prognosis and survival in NSCLC patients. Our data indicates that RUMI modulates Notch activity in NSCLC cells, and that its silencing dramatically decreases cell proliferation, migration and survival. RUMI downregulation causes severe cell cycle S-phase arrest, increases genome instability, and induces late-apoptotic/non-apoptotic cell death. Our studies demonstrate that RUMI is a novel negative prognostic factor with significant therapeutic potential in NSCLC, which embodies particular relevance especially when considering that while current Notch

Corresponding author: Dr. Rodrigo Fernandez-Valdivia, Department of Pathology, Wayne State University School of Medicine, 540 E. Canfield, Room 9248, Detroit, MI 48201, Phone: 313-577-0879, FAX: 313-577-0057, rcfernan@med.wayne.edu.

Conflict of Interest

The authors declare that they have no conflicts of interest

inhibitory strategies target only ligand-dependent Notch activation, a large number of NSCLCs are driven by ligand-independent Notch activity.

Keywords

Non-Small Cell Lung Cancer; Notch Signaling; RUMI; POGLUT1

Introduction

Notwithstanding the enormous progress made in the dissection of the signaling pathways and networks governing lung development and carcinogenesis (Johnson et al., 2001; Richer et al., 2015; Unni et al., 2015), and the substantial advances in the identification of lung cancer driver mutations (Bauml et al., 2013; Luo and Lam, 2013; Thompson et al., 2016), the precise molecular and cellular mechanisms triggering lung cancer initiation and formation are not yet clearly understood. Remarkably, recent comprehensive next-generation genome and transcriptome analyses in lung cancer patients (Campbell et al., 2016; Schwaederle et al., 2015; Xu et al., 2016), numerous basic and clinical studies (Chang et al., 2016; Dang et al., 2000; Donnem et al., 2010; Konishi et al., 2010; Kuramoto et al., 2012; Lin et al., 2010; Yang et al., 2011; Yuan et al., 2015), and compelling evidence from mouse models of lung cancer (Ambrogio et al., 2016; Maraver et al., 2012; Osanyingbemi-Obidi et al., 2011; Xu et al., 2014; Zheng et al., 2013) have uncovered a critical role for Notch signaling in lung cancer initiation and progression.

Notch is an evolutionarily conserved cell-to-cell signaling pathway that is widely used by metazoans during development and in the maintenance of adult homeostasis (Jafar-Nejad et al., 2010; Kopan and Ilagan, 2009; Ntziachristos et al., 2014), and is crucial in the regulation of important biological processes including cell proliferation, differentiation, asymmetric cell division, cell fate specification, compartment boundary formation, and lateral inhibition (Carlson and Conboy, 2007; Chiba, 2006; Fortini, 2009; Kopan and Ilagan, 2009; Regan et al., 2013; Tien et al., 2009; Wang et al., 2009). In its canonical mode of activation, Notch signaling is initiated when transmembrane Notch receptors (Notch1, 2, 3 and 4) on “signal-receiving cells” interact with transmembrane ligands of the Delta (Delta-like1, 3 and 4) and Serrate/Jagged (Jagged1 and 2) families on apposed “signal-sending cells” (Guruharsha et al., 2012; Jafar-Nejad et al., 2010; Kopan and Ilagan, 2009). Upon ligand binding, Notch receptors undergo a series of sequential proteolytical cleavages catalyzed by ADAM10/17 proteases (S2 site) and the γ-secretase complex (S3/S4 sites), which, eventually, cause the release of the Notch intracellular domain (NICD) and its consecutive translocation to the cell nucleus, where it participates in a transcriptional activator complex along with CSL (Rbpjk) and Mastermind proteins to activate the expression of downstream target genes (Guruharsha et al., 2012; Jafar-Nejad et al., 2010; Kopan and Ilagan, 2009). Notably, the Notch pathway is modulated at various levels including Notch receptor maturation and post-translational modification, ligand binding, and proteolytical processing (Jafar-Nejad et al., 2010; Kopan and Ilagan, 2009), and some of these regulatory mechanisms can be used as vulnerable points to block Notch signaling activity in human malignancies (Purow, 2012). However, current Notch inhibitory therapies have severe side effects (Krop et al., 2012; Schott et al.,

2013; Tolcher et al., 2012), are poorly selective (Lleo, 2008), and target only canonical, ligand-dependent Notch signaling.

While the presence of *O*-glucose glycans on the extracellular surface of Notch receptors has been known for some time (Moloney et al., 2000), the biological significance of these glycans on Notch activity was only recently established after the identification of Rumi in *Drosophila* (Acar et al., 2008) and mice (Fernandez-Valdivia et al., 2011). Rumi (Poglut1) is a CAP10 domain-containing, KDEL-like "protein *O*-glucosyltransferase" that resides in the Endoplasmic Reticulum (Acar et al., 2008; Fernandez-Valdivia et al., 2011; Leonardi et al., 2011; Takeuchi et al., 2011) and regulates Notch signaling through *O*-glucosylation of specific serine residues located within discrete EGF repeats present in the extracellular domain of Notch receptors (Acar et al., 2008; Fernandez-Valdivia et al., 2011; Leonardi et al., 2011). Notably, Rumi is the sole enzyme capable of *O*-glucosylating Notch receptors in humans (Fernandez-Valdivia et al., 2011; Takeuchi et al., 2011), and Notch receptors are the main targets of Rumi (Acar et al., 2008; Fernandez-Valdivia et al., 2011; Leonardi et al., 2011). Remarkably, Rumi regulates Notch signaling activity in a dosage-dependent manner (Fernandez-Valdivia et al., 2011; Leonardi et al., 2011), and modulates canonical Notch signaling at a molecular step mapped between ligand binding and the S3 cleavage (Acar et al., 2008; Fernandez-Valdivia et al., 2011; Leonardi et al., 2011). Strikingly, Rumi is also required for ligand-independent S2 cleavage activation of Notch (Leonardi et al., 2011), and its inactivation is capable of suppressing both hyperactive, ligand-independent Notch signaling activity and Notch activity-driven neoplastic cell growth (Leonardi et al., 2011).

In this research work, we used a combined approach utilizing gene and protein expression analyses in murine and patient specimens, comprehensive association studies between RUMI expression levels and Non-Small Cell Lung Cancer (NSCLC) patients' progression and survival, and gene silencing and cell functional assays in NSCLC cell culture systems to define the involvement of RUMI in the development and prognosis of NSCLC as well as to evaluate the therapeutic potential of its targeting.

Materials and Methods

Animals and cell lines

C57BL6/J mice were used for studies involving mouse specimens. For Rumi expression analysis in developing lung, mouse embryos sections corresponding to embryonic stages E11.5 to E18.5 were used. For Rumi expression analysis in adult lung, 8-week old mice were sacrificed and the left lung collected for histology processing. A549 (ATCC CCL-185) and H23 (ATCC, CRL-5800) cell lines were obtained from Dr. Jiang Wang and Dr. Menq-Jer Lee, respectively, and were authenticated through Short Tandem Repeat (STR) DNA profiling in Karmanos Cancer Institute's Biobanking and Correlative Sciences Core. Cells were grown in DMEM containing 10% fetal bovine serum. Puromycin was used as positive selector for establishing stably-transfected cell lines, at 0.75 μg/ml for H23 cells and 1.5 μg/ml for A549. Animal studies were approved by our Institutional Animal Care and Use Committee.

Tissue microarrays

NSCLC tissue microarrays were obtained from US Biomax. For AQUA analysis and patients' progression and survival studies, Karmanos Cancer Institute NSCLC tissue microarrays (KTMA) and Yale Cancer Center NSCLC tissue microarrays (YTMA) were used.

cBioportal data mining analysis

Searches in cBioportal (Cerami et al., 2012; Gao et al., 2013) for *RUMI* genetic alterations for human cancers were done using gene name *POGLUT1*. Searches were conducted for cancer genomic data in 164 studies and the results from the top-20 studies showing the highest frequency and absolute counts on genomic alterations in *RUMI* were selected.

Antibodies, immunoreagents and shRNAs

Two different Rumi antibodies were used for expression analyses. A validated rabbit polyclonal antibody against mouse Rumi (Fernandez-Valdivia et al., 2011) was used for immunodetection of Rumi in murine specimens, and a rabbit polyclonal antibody against mammalian Rumi (NBP1-90311, Novus Biologicals), and with reactivity to human RUMI (Basmanav et al., 2014), was used in human samples. A rabbit polyclonal antibody was used for detection of surfactant protein C (SP-C) (AB3786, EMD Millipore) and a goat polyclonal antibody was used for Club cell secretory protein (CCSP) (sc-9772, Santa Cruz Biotechnologies). Alexa488-conjugated donkey anti-rabbit (711-545-152), Alexa488-conjugated donkey anti-goat (705-545-147), Cy3-conjugated donkey anti-rabbit (711-165-152), and donkey anti-rabbit Fab-fragment (711-007-003) were obtained from Jackson Immunoresearch. For AQUA analysis, the pan-Cytokeratin mouse antibody (clone AE1/AE3, M3515) and the polymer-HRP anti-rabbit solution (K4011) were from DAKO Cytomation, and the Alexa555-conjugated goat anti-mouse (821424) was from Life Technologies. Non-target control MISSION shRNA (SHC002) and the two independent and non-overlapping MISSION shRNAs directed against two distinct regions of the coding sequence of human *RUMI* mRNA (shRNA1, TRCN0000155317; shRNA2, TRCN0000151420) were from SIGMA. Plasmids containing the distinct shRNAs were used for transfection and subsequent generation of stably-transfected cell lines.

Immunohistochemistry, immunofluorescence, AQUA analysis

For immunohistochemistry and dual immunofluorescence stainings, antigen was retrieved by heat-induced epitope retrieval in citrate buffer and sections were blocked with 3% normal donkey serum. For immunohistochemistry experiments, Vectastain ABC kit (PK-4001, Vector Laboratories) and ImmPACT DAB substrate (SK-4105, Vector Laboratories) were used for chromogenic reactions along with hematoxylin counterstaining. Dual immunofluorescence experiments were done sequentially, and two blocking steps with normal rabbit serum and donkey anti-rabbit Fab fragments were done after the first immunoreaction in Rumi and SP-C dual immunofluorescence experiments.

For Rumi immunofluorescence in cultured cells, 3×10^5 cells were plated in coverslips and grown for 24h. Samples were fixed in 4% formaldehyde, permeabilized with 0.01% Triton X-100, and blocked with 3% normal donkey serum. The coverslips were then incubated

overnight with primary antibody followed by three washes in PBS and a 2h incubation with the secondary antibody. Samples were mounted with Antifade Mounting Medium with DAPI (H-1200, Vector Laboratories) and the images were acquired in a Leica microscope using Spot Imaging Software 5.1 (Diagnostic Instruments).

Dual immunofluorescence stainings for AQUA analysis were done using heat-induced epitope retrieval in citrate-based Unmasking Solution (H-3300, Vector Laboratories) and a 15-min incubation with Background Sniper (BS966, Biocare) for blocking unspecific binding. RUMI and cytokeratin immunoreactions were done simultaneously, and RUMI was detected using Cy5 tyramide chemistry (SAT705A001EA, Perkin-Elmer). Slides were mounted in Prolong Gold antifade reagent with DAPI (P36931, Thermo Fisher) and allowed to cure overnight before imaging acquisition. Tissue microarray slides were scanned and core images were acquired and scored using an AQUA system (PM-2000, version 2.3.4.1, Genoptix). Exported images were pseudocolored using green color for Alexa-555 signals (cytokeratins staining) and red color for Cy5 signals (RUMI staining).

Statistical analyses for RUMI 's prognostic role in NSCLC

The primary objective was to assess the independent prognostic role of RUMI in NSCLC patients. The primary clinical endpoint was the Overall Survival (OS) defined as time from diagnosis to death of any cause. The secondary clinical endpoint was the time to progression (TTP) defined as time from diagnosis to documented date of progression or death due to disease progression. Two independent cohorts, KTMA and YTMA, were used as training and validation sets, respectively. Expression measurements from KTMA with AQUA were dichotomized into high/low status and evaluated with log-rank tests for OS. The optimal cut-off was defined as cut-off that resulted with the lowest log-rank *P* value, and it was further validated with multivariate Cox model in the training set and validation set adjusted for age, gender, tumor stage, and histology. As tumor stage is a well-known prognostic factor, Kaplan-Meier (KM) plot of OS in the validation set based on protein expression high/low status was stratified on tumor stage. Associations between the protein high/low status and baseline patient characteristics were tabulated and tested with Fisher's exact test or Wilcoxson test as appropriate. All statistical tests were two-sided and *P* values less than 0.05 were considered significant. Statistical analyses were performed using R v3.3 (The R Foundation for Statistical Computing).

RT-qPCR

Total RNA was extracted using TRIZOL (Life Technologies) and RNeasy micro columns (QIAGEN) following manufacturer instructions. RNA was quantified using a DeNovix DS-11 nano spectrophotometer (DeNovix). Samples were diluted in nuclease-free water and 100 ng total RNA per well were used in RT-qPCR experiments using One-Step RT-qPCR master mix (Life Technologies). Validated Taqman hydrolysis assays were obtained from Life Technologies and included primers/probe sets for *RUMI* (Hs00220308_m1), *HEY1* (Hs01114113_m1), *HES2* (Hs00219505_m1) and 18S rRNA (4319413E). RT-qPCR experiments were conducted in a Lightcycler 96 qPCR instrument (Roche) and Cq values were automatically calculated by the instrument software without user intervention. Obtained Cq values were used for estimating relative expression levels with the $2^{-\Delta\Delta Cq}$

method and using 18S rRNA as reference. Three independent biological replicates and two independent technical replicates per experiment were used. Statistical analysis of the data was performed using two-tail Student's t-test.

Wound healing (scratch) assays

Cells (1×10^6 per well) were plated in 24-well plates and cultured until cells settled and were confluent. A scratch in the cell monolayer was made with a 200 μl pipette tip and micro photographs were taken, under phase contrast, immediately (0h time-point) and 24h after wounding. The area size of the wound was measured from the microphotographs and compared appropriately. Three independent replicates per experiment were used. Statistical analysis of the data was performed using two-tail Student's t-test.

Cell proliferation and cell death assays

For cell proliferation assays, single cells (trypsinized and passed through a 35 μm strainer) were cultured in 6-well plates at a density of 17,000 cells/well. Cells were grown for 1 to 9 days, fixed with 4% formaldehyde in PBS for 15 min, and stained with 0.1% crystal violet solution. After photographic documentation, 1 ml of 10% acetic acid was added to each well and the resulting solution was diluted in water for determining absorbance at 590 nm. Dilutions were made such that the absorbance of the sample with lowest transmittance (highest absorbance) was below one. Annexin-V cell death apoptosis assays were done using Annexin-V Dead Cell Apoptosis system (V13241, Life Technologies) and following manufacturer instructions. Flow cytometry was carried out in a BD LSR II flow cytometer and data was analyzed with FlowJo v10 software (FlowJo). Three independent replicates per experiment were used in these studies. Statistical analysis of the data was performed using two-tail Student's t-test.

Cell Cycle Analyses

For DAPI/EdU incorporation analysis, cells were grown in 6-well plates until 60-80% confluency. Cells were administered with EdU (Click-iT EdU kit, C10425, Thermo) and allowed to incorporate EdU for 2h, after which cells were fixed and labeled according to manufacturer instructions. Flow cytometric analysis was carried out in a BD LSR II flow cytometer and FlowJo v10 software (FlowJo) was used for data analysis. For high-resolution DAPI and DNA ploidy cell cycle analysis (DAPI assay/ModFit modeling), $1\text{-}5\times10^6$ single cells were resuspended in paraformaldehyde-based fixation buffer (Click-iT EdU kit, C10425, Thermo) and fixed for 15 min. Fixed cells were stained with DAPI (1 mg/ml in 0.1% Triton X-100 in PBS), washed in PBS and analyzed with a BD LSR II flow cytometer and ModFit LT v4.0 software (Verity).

Results

Rumi is expressed in the alveolar and bronchiolar epithelia and its expression is developmentally controlled

To begin exploring the role of Rumi in lung biology and function, we first performed a series of immunohistochemistry experiments to determine Rumi expression patterns in the developing and adult murine lung. Our Rumi immunohistochemistry studies in distinct

embryonic and fetal lung developmental stages indicate that Rumi expression is dynamically controlled in the developing lung epithelium. Specifically, we found that Rumi expression becomes noticeable in the primitive lung epithelium at E11.5 late embryonic stage (Fig. 1A), and that its expression progressively increases in both the proximal and distal endoderm-derived lung epithelium during the pseudoglandular stage (E12.5-15.5). Interestingly, Rumi expression levels do not follow a steady increase dynamics during the subsequent phases of lung development. While Rumi levels reach a maximum at developmental stage E15.5, it starts decreasing—though showing a relatively more scattered pattern in the distal lung—during the canalicular (E15.5-E17.5) and saccular (E18.5) stages (Fig. 1A).

To determine the cellular pattern/profile of Rumi expression in the pulmonary epithelium, we performed Rumi immunohistochemical experiments and colocalization studies in murine adult lung. Our immunostainings indicated that Rumi was present in both the bronchiolar and alveolar epithelia, and with a marked scattered expression pattern in the alveolar parenchyma (Fig. 1B). Due to their important role in lung carcinogenesis (Cho et al., 2011; Mainardi et al., 2014; Sutherland et al., 2014; Unni et al., 2015; Xu et al., 2012), we then investigated whether among the cells expressing Rumi were alveolar type II cells and bronchiolar Club cells (formerly Clara cells), for which we performed dual immunofluorescence stainings with surfactant protein C (SP-C) and Club cell secretory protein (CCSP). Our data on dual immunofluorescence stainings for Rumi and SP-C revealed that cells stained positive for SP-C were also positive for Rumi (Fig. 1C), indicating that Rumi is expressed in type II pneumocytes. Notably, through this colocalization experiment, it was evident that Rumi is not exclusively expressed in alveolar type II cells since there were also cells in the alveolar parenchyma that scored positive for Rumi but not for SP-C (Fig. 1C). Our results on Rumi and CCSP dual immunofluorescence experiments showed that cells stained positive for CCSP scored also positive for Rumi (Fig. 1D), allowing us to conclude that Rumi is expressed in Club cells. Collectively, these studies demonstrate that Rumi is expressed in both alveolar type II cells and bronchiolar Club cells.

RUMI is amplified and highly overexpressed in Non-Small Cell Lung Cancer

To investigate the possible implication of RUMI in NSCLC, we searched for recurrent chromosomal aberrations in NSCLC and the presence of genomic alterations in *RUMI* in NSCLC. Remarkably, our searches indicate that *RUMI* maps to chromosome 3q13.33 (Fig. 2A), which is within a region that corresponds to the major signature of neoplastic transformation in NSCLC (Balsara, 1997; Perterson, 1997), suggesting that *RUMI* could thus be implicated in NSCLC development. Accordingly, our inquiries in biorepository databases of genomic alterations in human cancers (Cerami et al., 2012; Gao et al., 2013) indicated that the frequency of *RUMI* amplifications is markedly high in NSCLC, including, in particular, the Squamous Cell Carcinoma subtype (Fig. 2A). Indeed, so far the largest number of cases in which *RUMI* amplifications have been found correspond to NSCLC (Fig. 2B).

To confirm this genomic data, we decided to examine the expression of RUMI in NSCLC tumor subtypes. Our RUMI immunohistochemical analyses in NSCLC microarray panels containing 142 tissue cores indicate that, in comparison to normal lung parenchyma, RUMI

is significantly elevated in NSCLC. Concretely, we found that RUMI levels were significantly increased by 2-3 fold in distinct subtypes of NSCLC including adenocarcinoma (2.4 fold), squamous cell carcinoma (3.2 fold), adenosquamous cell carcinoma (3.2 fold), bronchioalveolar carcinoma (3.1 fold), and large cell carcinoma (2.4 fold) (Fig. 2C). Of note, this observed relative increase in the expression of RUMI in tumor cells was also noticed with respect to tumor-surrounding stromal tissue, and many mitotically active cells seen in tumors displayed high levels of RUMI expression (Fig. 2C). Together, these results indicate that *RUMI* is markedly amplified and overexpressed in NSCLC tumors.

RUMI is a novel negative prognostic marker in NSCLC

To further evaluate the potential predictive value of RUMI in NSCLC we performed an assessment of RUMI expression in lung adenocarcinoma and squamous cell carcinoma tumor types and determined its association with patients' prognosis and survival. We used a fluorescence-based immunohistochemistry method combined with automated quantitative analysis (AQUA) for assessing RUMI expression levels in Karmanos Cancer Institute NSCLC training tissue microarrays (KTMA) and Yale Cancer Center NSCLC validation tissue microarrays (YTMA) (representative images in Fig. 3A, B). We identified an optimal threshold from KTMA for the primary endpoint OS (AQUA=11,134) from this training data, and it was afterwards validated with Cox multivariable model with OS and TTP (see Fig. 3C and below). As can be seen in the table inscribed in Figure 3C, patients with high levels of RUMI expression in the KTMA cohort had worse OS prognosis, with a statistically significant increase in the hazard ratio (HR) value (HR=1.81, 95% CI (1.08 to 3.01), P=0.023). Critically, these results were further validated in the YTMA cohort, where patients with high RUMI expression also show worse OS prognosis (HR=2.89, 95% CI (1.17 to 7.16), P=0.022). Importantly, we found no association between the high/low status of RUMI and known prognostic factors (Fig. S2A, B), indicating that RUMI is, indeed, an independent prognostic factor in lung adenocarcinoma and lung squamous cell carcinoma.

To conduct a more in-depth scrutiny of our data, we also performed a stratified KM analysis for RUMI expression and OS in the validation YTMA cohort (Fig. 3D). Notably, our results in this study indicated that while the Median OS for Stage I patients and low RUMI expression was 7.757 years 95% CI (4.74 ~NA), the Median OS for Stage I patients and high RUMI expression was 2.66 years 95% CI (2.14 ~NA). Likewise, whereas Stage >I patients with low RUMI expression had a Median OS of 2.11 years 95% CI (1.75 ~ 4.91), Stage >I patients with high RUMI expression had a Median OS of 0.711 years 95% CI (NA~NA) (Fig. 3D). In congruity, our results reveal that patients with high RUMI levels in the TNM Stage I group have a statistically significant increase in HR (2.71, P=0.039) with respect to patients with low RUMI levels, and that patients with high RUMI levels in the TNM Stage >I group had a highly statistically significant increase in HR (11.99, P=0.005) in comparison to patients with low levels of RUMI expression (Fig. 3D). Furthermore, our multivariable Cox analysis for TTP in KTMA indicates that patients with high levels of RUMI expression have a highly significant increased HR of 2.32 (95% CI (1.48 to 4.27), P=0.008) compared to patients with low levels of RUMI. Taken together, our data indicates that RUMI expression levels have a strong predictive value for disease progression and poor

survival, and affirmatively supports the utility of RUMI as novel biomarker in the prognosis of lung adenocarcinoma and lung squamous cell carcinoma.

RUMI regulates Notch signaling activity in NSCLC cells

Given that Rumi has been shown to modulate Notch signaling activity (Acar et al., 2008; Fernandez-Valdivia et al., 2011; Leonardi et al., 2011), and considering recent findings demonstrating Notch signaling involvement and requirement in NSCLC development (Allen et al., 2011; Ambrogio et al., 2016; Licciulli et al., 2013; Maraver et al., 2012; Xu et al., 2014; Zheng et al., 2013), we decided to investigate RUMI's regulation of Notch activity in NSCLC cell lines. To this end, we employed an RNAi-mediated *RUMI* genetic silencing approach combined with Notch signaling readout evaluation in A549 and H23 NSCLC cells (Fig. 4). We first performed validation of several shRNAs directed against the coding region of human *RUMI* mRNA, which resulted in the identification of two distinct shRNAs (onwards referred to as shRNA1 and shRNA2) that effectively silence *RUMI* expression (Fig. S3). Our RT-qPCR and immunofluorescence analyses indicate that these shRNAs were effective in silencing *RUMI* in both A549 and H23 NSCLC cells, as evidenced by the highly statistically significant decrease (65.6% by shRNA1 and 74.7% by shRNA2) in *RUMI* mRNA levels in A549 cells (Fig. 4A), and the marked absence of RUMI immunoreactivity in H23 cells (Fig. 4B). As expected, *RUMI* knockdown in A549 cells resulted in a highly significant decrease in transcript levels of Notch effectors *HEY1* (61.3% by shRNA1 and 70.7% by shRNA2), and *HES2* (60.2% by shRNA1 and 53.9% by shRNA2), thus indicating that *RUMI* silencing downregulates Notch signaling activity in these cells (Fig. 4A). Similarly, *RUMI* silencing in H23 cells caused significant and highly significant decreases in mRNA levels of Notch downstream targets *HEY1* (46.3% by shRNA1 and 44.2% by shRNA2), and *HES2* (43.3% by shRNA1 and 37.3% by shRNA2) (Fig. 4C). In conclusion, these results indicate that RUMI silencing could effectively inhibit Notch signaling activity in NSCLC cell lines.

RUMI is required for cell proliferation, migration and survival in NSCLC

Having demonstrated Notch signaling inhibition through *RUMI* silencing, we next explored the effects of *RUMI* knockdown on cell function in NSCLC cell lines. Our data on crystal violet assays indicate that *RUMI* silencing dramatically affects cell proliferation of A549 cells (Fig. 5A, B). Concisely, we observed that in comparison to A549 Non-target control cells, 1.9-fold and 2.5-fold differences in absorbance levels (proportional to cell number) were seen in *RUMI*-silenced cells (with either shRNA1 or 2) at 7- and 9-day time-points, respectively (Fig. 5A, B).

To investigate the potential cellular mechanism underlying the observed cell proliferation defects in RUMI deficient NSCLC cells, we performed DAPI and DAPI/EdU incorporation assays in *RUMI*-silenced A549 cells along with high-resolution DAPI/DNA ploidy cell cycle analysis in *RUMI*-silenced H23 NSCLC cells. The results of our DAPI and DAPI/EdU incorporation experiments clearly show that *RUMI* knockdown causes a severe S-phase arrest in A549 cells (Fig. 5C, D and Fig. S4A, B), with a highly statistically significant increase in the fraction of cells actively incorporating EdU into their DNA, from 28.1% in Non-target control cells to 39.7% and 48.2% in *RUMI*-silenced cells with shRNA1 and

shRNA2, respectively (Fig. 5D). It is important to note that the requirement of RUMI's function in cell cycle progression was also observed in H23 cells (Fig. 5E, F), which, similarly to what was shown for A549 cells, show a statistically significant increase in the proportion of total S-phase arrested cells (46.4% in shRNA1 and 42.3% in shRNA2 compared to 40.1% in Non-target shRNA) (Fig. 5F). Interestingly, in H23 cells, a further marked aneuploid genomic instability was also observed upon *RUMI* knockdown (modeled as aneuploid, An1, in Fig. 5E), and the fraction of S-phase arrested cells was significantly higher also when analyzed separately in both cycling cells (algorithmically modeled as diploid, Dip, in Fig. 5E to facilitate comparison) and further aneuploid cells with increased DNA content (modeled as An1 in Fig 5E) (Fig. S4C, D), indicating that *RUMI* deficiency prevents cells from division and causes an accumulation of cells undergoing DNA synthesis and increasing their DNA content. Given that cell proliferation defects can also be explained by changes in cell death rate, we also conducted cell apoptosis assays in A549 *RUMI*-silenced cells. Interestingly, our Annexin-V/propidium iodide assays showed that *RUMI* silencing did not result in increased numbers of cells undergoing early apoptosis (Fig. 5G), but, nevertheless, caused a strikingly distinguishable increase in the fraction of cells undergoing late-apoptotic/non-apoptotic cell death (Fig. 5G, H), with a statistically significant 2.5% in shRNA1-stably transfected cells and a highly statistically significant 2.4% in shRNA2-stably transfected cells compared to 1.7% in Non-target control A549 cells (Fig. 5H).

To further investigate the effects that decreased RUMI expression has on NSCLC cell function, we also studied cell migration using wound healing assays in A549 and H23 *RUMI*-silenced cells. Our data in these studies manifestly show that RUMI silencing results in a marked impairment on cell migration in both H23 and A549 cells (Fig. 5I, J and Fig. S4E, F). We observed that while H23 Non-target control cells covered 71% of the wounded area after a 24-hour time interval, *RUMI*-silenced cells covered only 30% (shRNA1) and 46% (shRNA2) (Fig. 5I, J). Similarly, our data on A549 cells, indicates that a statistically significant difference in the wound healing capacity is exhibited in *RUMI* knockdown cells (42% in shRNA1 and 46% in shRNA2) compared to Non-target control cells (78%) (Fig. S4E, F). All together, our results demonstrate that RUMI function is required for NSCLC cell proliferation, genome stability, migration and survival.

Discussion

Studies on Notch signaling's role in lung morphogenesis indicate that this pathway primarily controls cell fate decisions (Morimoto et al., 2010; Morimoto et al., 2012; Tsao et al., 2009) and is necessary for proper alveolar formation (Tsao et al., 2016; Zhang et al., 2013). Targeted inactivation of either *Rbpjk* or *Jagged1* in the pulmonary epithelium results in alveolarization and septation defects (Xu et al., 2010; Zhang et al., 2013), and Notch2 is required for alveolar type II cell proliferation and maturation (Tsao et al., 2016). Moreover, *Shh-Cre*-directed deletion of Notch regulator *Pofut1* (protein *O*-fucosyltransferase 1) causes a marked decrease in type II cell proliferation and failure in alveolarization accompanied by emphysematous enlargement of the distal airspaces (Tsao et al., 2016). Within this context, our findings indicating that central Notch signaling regulator Rumi is markedly and dynamically expressed in the pulmonary epithelium, could plausibly support a role for this

enzymatic modulator in the control of Notch activity during lung morphogenesis and in the maintenance of adult lung homoeostasis. Our results clearly indicate that Rumi is expressed in the developing lung epithelium, becoming noticeable at E11.5 and progressively increasing until E15.5, a stage at which a marked peak in its expression is observed. Interestingly, it should be pointed out that Notch receptors, as well as Notch ligands Dll1 and Jagged1, have also been observed to become progressively expressed from E11.5 onwards (Ito et al., 2000; Taichman et al., 2002), although, and in contrast to Rumi, their expression levels steadily increase to adulthood (Ito et al., 2000; Taichman et al., 2002). Nonetheless, our data also indicates that Rumi expression becomes seemingly more restricted to the proximal and/or bronchiolar epithelium during late stages of fetal development (E16.5 - E18.5), and acquiring a more scattered pattern in the distal lung which, while could compound precise assertion of its levels in the developing lung, could also, conceivably, relate these differing observations. Noticeably, our immunostainings in murine adult lung showed that Rumi is expressed in Club cells and type II pneumocytes, although the expression on these latter cells in the alveolar parenchyma was not exclusive and other cell types like type I pneumocytes and myofibroblasts could also be expressing Rumi. Of importance, it is shown that Notch1 over-activation in SP-C-expressing cells results in mucous metaplasia and reduction of ciliated cells (Guseh et al., 2009), and that Notch signaling abrogation disrupts Club cell fate specification, causing an imbalance towards the generation of ciliated cells (Morimoto et al., 2010; Morimoto et al., 2012; Tsao et al., 2016; Tsao et al., 2009; Zhang et al., 2013). While our studies in this subject are limited and cannot provide an assessment of Rumi's function on type II cells or Club cells, our data from gene silencing experiments in A549 and H23 lung cancer cells showing a requirement for RUMI in Notch activity and cell proliferation and survival, could certainly support the notion that RUMI could be exerting a functional role in these cell populations. Future work with cell-targeted *Rumi* gain- and loss-of-function studies will be necessary to ascribe its Notch regulatory role in type II cells and Club cells and determine its functional importance in lung development and homeostasis.

The involvement of Notch signaling in lung carcinogenesis was first recognized when a somatic chromosomal translocation t(15;19), causing overexpression of the *Notch3* gene, was discovered in poorly differentiated aggressive lung carcinoma (Dang et al., 2000). Remarkably, activating mutations in Notch1 heterodimerization and PEST domains have been found in 10% NSCLCs (Westhoff et al., 2009), and elevated Notch3 expression has been shown to occur in 30-40% of primary lung tumors (Haruki et al., 2005). Moreover, loss of Numb, a negative regulator of Notch, is found in 30% of NSCLC cases, and targeted overexpression of the activated form of Notch1 (N1ICD) in the pulmonary epithelium causes alveolar hyperplasia and adenoma formation (Allen et al., 2011). In this study, we have found that *RUMI* is markedly amplified and overexpressed in several subtypes of NSCLC tumors, and that its expression levels significantly correlate with poor prognosis in TTP and OS in lung adenocarcinoma and lung squamous cell carcinoma patients. In this respect, we would first like to highlight the realization that *RUMI*'s chromosomal location in 3q13.33, and its amplification observed in NSCLCs in the cBioportal repository, seemingly corresponded to precognizant observations on comparative genomic hybridization analyses indicating that chromosome 3q13-qter is a region frequently altered in NSCLCs (Balsara et

al., 1997; Petersen et al., 1997), with specific marked amplifications in 3q13, 3q26 and 3q28-qter (Balsara et al., 1997). Secondly, we would like to point out that our results on protein expression analyses in various NSCLC tissue microarrays highly correlate with the above-mentioned genomic data and, thus, not only define *RUMI* as a novel amplified and overexpressed gene in NSCLC, but also very much confirm 3q13-qter as a major region for malignant transformation in NSCLC. Finally, we would like to emphasize the significance of our findings on RUMI's impact on patients' disease progression and OS, where increased levels of RUMI expression are associated with significantly elevated HRs, even within subgroups of TNM Stage I and TNM Stage >I, where the HRs reach dramatic values of 2.71 and 11.99, respectively, and the Median OS times are of only 2.11 and 0.711 years, and, thus, confirm RUMI's usefulness as a novel biomarker in NSCLC prognosis and survival. Of importance, previous studies on gene expression association analyses in NSCLC have also found significant correlations between expression and/or activation of Notch pathway components, including Notch1, Notch3, Dll4 and Jagged1, and worsen patients' disease progression and survival (Campbell et al., 2016; Chang et al., 2016; Donnem et al., 2010; Xu et al., 2016; Yuan et al., 2015; Zhou et al., 2013). In this respect, we could say that our work not only serves to reaffirm an association between Notch signaling activity and NSCLC development and poor prognosis, but, importantly, also allows us to conclude that RUMI is a novel strong independent prognostic factor for accelerated disease progression and poor survival in NSCLC patients.

Notch signaling inhibition has recently emerged as a novel therapeutic modality to treat human malignancies, and a number of clinical trials with Notch activity inhibitors in patients with solid tumors have shown that pharmacological inhibition of Notch is a promising therapeutic strategy (Krop et al., 2012; Schott et al., 2013; Tolcher et al., 2012). Moreover, it is known that Notch3 blockade impairs the self-renewal capacity of $CD24^{+}ITGB4^{+}Notch^{hi}$ NSCLC tumor-initiating cells (Zheng et al., 2013), and that Notch activity is required for Kras-induced adenocarcinoma development (Allen et al., 2011; Licciulli et al., 2013; Maraver et al., 2012; Xu et al., 2014). Strikingly, inactivation of *presenilins 1* and *2*, disruption of the canonical Notch activation-mediator *Rbpjk*, or pharmacological inhibition of the γ-secretase complex, all exert a suppressive effect on Kras-driven lung adenocarcinoma development (Maraver et al., 2012). Our present work on RUMI's regulation of Notch signaling in NSCLC cell lines indicates that RUMI is clearly required for Notch signaling activation, and that in its absence marked defects in cell proliferation, migration, genome stability, and survival are displayed. Consequently, our results are in line with the idea that RUMI, and hence Notch signaling, has a tumor growth-promoting role in NSCLC, and that targeting RUMI could possibly offer a novel therapeutic avenue for attaining Notch signaling inhibition in NSCLCs. In this respect, it is important to note that while regulatory nodes controlling Notch activity are currently being used as vulnerable points to block Notch signaling activation (Purow, 2012), with strategies including small molecule γ-secretase inhibitors and blocking antibodies against Notch receptors or ligands (Brennan and Clarke, 2013; Purow, 2012), these therapies are notorious for showing severe side effects, having poor selectivity, and targeting only ligand-dependent Notch signaling activity (Krop et al., 2012; Lleo, 2008; Schott et al., 2013; Tolcher et al., 2012). In this aspect, Rumi has been shown to not only act as an essential enzyme for canonical Notch

signaling activity (Acar et al., 2008; Fernandez-Valdivia et al., 2011; Leonardi et al., 2011), but also to be critical for ligand-independent S2 cleavage activation of Notch receptors (Leonardi et al., 2011). Furthermore, Rumi inactivation has been shown to be effective in suppressing both oncogenic Notch$^{\Delta LNR}$ hyperactivity and Notch activity-driven neoplastic cell growth (Leonardi et al., 2011), which, in the context of NSCLC is of particular importance, especially considering that many NSCLCs are driven by ligand-independent Notch activity (Westhoff et al., 2009). In conclusion, our observations indicate that RUMI could conceivably be an actionable driver in NSCLC, and that its targeting could entail great therapeutic potential not only for Notch activity-driven NSCLCs, but also for the devising of future synthetic lethality-based combinational therapies.

Supplementary Material

Refer to Web version on PubMed Central for supplementary material.

Acknowledgments

We would like to thank Jian Wang and Menq-Jer Lee for kindly providing NSCLC cell lines, and Daniel Bonfil for his critical and constructive scientific advises. We would also like to thank Jessica Back and Eric van Buren for outstanding assistance in flow cytometry experiments and analyses. Thanks are also extended to Olga Mejia, Ruta Jog and Iosif Barjuca for excellent laboratory assistance.

This work has been supported by Wayne State University's Startup Funds and Grant Boost Award, Karmanos Cancer Institute (KCI) and McLaren Infrastructure and Initiative Awards, and by the American Cancer Society and KCI ACS-IRG Awards 11-053-01-IRG and 14-238-04-IRG (RFV). This work was also supported by an NIH CCSG grant (P30CA022453) (GB and WCh). The Microscopy, Imaging and Cytometry Resources Core is supported, in part, by NIH Center grant P30CA22453 to The Karmanos Cancer Institute, Wayne State University and the Perinatology Research Branch of the National Institutes of Child Health and Development, Wayne State University.

References

Acar M, Jafar-Nejad H, Takeuchi H, Rajan A, Ibrani D, Rana NA, Pan H, Haltiwanger RS, Bellen HJ. Rumi is a CAP10 domain glycosyltransferase that modifies Notch and is required for Notch signaling. Cell. 2008; 132(2):247–258. [PubMed: 18243100]

Allen TD, Rodriguez EM, Jones KD, Bishop JM. Activated Notch1 induces lung adenomas in mice and cooperates with Myc in the generation of lung adenocarcinoma. Cancer Res. 2011; 71(18): 6010–6018. [PubMed: 21803744]

Ambrogio C, Gomez-Lopez G, Falcone M, Vidal A, Nadal E, Crosetto N, Blasco RB, Fernandez-Marcos PJ, Sanchez-Cespedes M, Ren X, Wang Z, Ding K, Hidalgo M, Serrano M, Villanueva A, Santamaria D, Barbacid M. Combined inhibition of DDR1 and Notch signaling is a therapeutic strategy for KRAS-driven lung adenocarcinoma. Nat Med. 2016; 22(3):270–277. [PubMed: 26855149]

Balsara BR, Sonoda G, du Manoir S, Siegfried JM, Gabrielson E, Testa JR. Comparative genomic hybridization analysis detects frequent, often high-level, overrepresentation of DNA sequences at 3q, 5p, 7p, and 8q in human non-small cell lung carcinomas. Cancer Res. 1997; 57(11):2116–2120. [PubMed: 9187106]

Basmanav FB, Oprisoreanu AM, Pasternack SM, Thiele H, Fritz G, Wenzel J, Grosser L, Wehner M, Wolf S, Fagerberg C, Bygum A, Altmuller J, Rutten A, Parmentier L, El Shabrawi-Caelen L, Hafner C, Nurnberg P, Kruse R, Schoch S, Hanneken S, Betz RC. Mutations in POGLUT1, encoding protein O-glucosyltransferase 1, cause autosomal-dominant Dowling-Degos disease. American journal of human genetics. 2014; 94(1):135–143. [PubMed: 24387993]

Bauml J, Mick R, Zhang Y, Watt CD, Vachani A, Aggarwal C, Evans T, Langer C. Frequency of EGFR and KRAS mutations in patients with non small cell lung cancer by racial background: do disparities exist? Lung cancer. 2013; 81(3):347–353. [PubMed: 23806795]

Brennan K, Clarke RB. Combining Notch inhibition with current therapies for breast cancer treatment. Therapeutic advances in medical oncology. 2013; 5(1):17–24. [PubMed: 23323144]

Campbell JD, Alexandrov A, Kim J, Wala J, Berger AH, Pedamallu CS, Shukla SA, Guo G, Brooks AN, Murray BA, Imielinski M, Hu X, Ling S, Akbani R, Rosenberg M, Cibulskis C, Ramachandran A, Collisson EA, Kwiatkowski DJ, Lawrence MS, Weinstein JN, Verhaak RG, Wu CJ, Hammerman PS, Cherniack AD, Getz G, Cancer Genome Atlas Research N. Artyomov MN, Schreiber R, Govindan R, Meyerson M. Distinct patterns of somatic genome alterations in lung adenocarcinomas and squamous cell carcinomas. Nature genetics. 2016; 48(6):607–616. [PubMed: 27158780]

Carlson ME, Conboy IM. Regulating the Notch pathway in embryonic, adult and old stem cells. Curr Opin Pharmacol. 2007; 7(3):303–309. [PubMed: 17475556]

Cerami E, Gao J, Dogrusoz U, Gross BE, Sumer SO, Aksoy BA, Jacobsen A, Byrne CJ, Heuer ML, Larsson E, Antipin Y, Reva B, Goldberg AP, Sander C, Schultz N. The cBio cancer genomics portal: an open platform for exploring multidimensional cancer genomics data. Cancer discovery. 2012; 2(5):401–404. [PubMed: 22588877]

Chang WH, Ho BC, Hsiao YJ, Chen JS, Yeh CH, Chen HY, Chang GC, Su KY, Yu SL. JAG1 Is Associated with Poor Survival through Inducing Metastasis in Lung Cancer. PloS one. 2016; 11(3):e0150355. [PubMed: 26930648]

Chiba S. Notch signaling in stem cell systems. Stem Cells. 2006; 24(11):2437–2447. [PubMed: 16888285]

Cho HC, Lai CY, Shao LE, Yu J. Identification of tumorigenic cells in Kras(G12D)-induced lung adenocarcinoma. Cancer Res. 2011; 71(23):7250–7258. [PubMed: 22088965]

Dang TP, Gazdar AF, Virmani AK, Sepetavec T, Hande KR, Minna JD, Roberts JR, Carbone DP. Chromosome 19 translocation, overexpression of Notch3, and human lung cancer. J Natl Cancer Inst. 2000; 92(16):1355–1357. [PubMed: 10944559]

Donnem T, Andersen S, Al-Shibli K, Al-Saad S, Busund LT, Bremnes RM. Prognostic impact of Notch ligands and receptors in nonsmall cell lung cancer: coexpression of Notch-1 and vascular endothelial growth factor-A predicts poor survival. Cancer. 2010; 116(24):5676–5685. [PubMed: 20737536]

Fernandez-Valdivia R, Takeuchi H, Samarghandi A, Lopez M, Leonardi J, Haltiwanger RS, Jafar-Nejad H. Regulation of mammalian Notch signaling and embryonic development by the protein O-glucosyltransferase Rumi. Development. 2011; 138(10):1925–1934. [PubMed: 21490058]

Fortini ME. Notch signaling: the core pathway and its posttranslational regulation. Developmental cell. 2009; 16(5):633–647. [PubMed: 19460341]

Gao J, Aksoy BA, Dogrusoz U, Dresdner G, Gross B, Sumer SO, Sun Y, Jacobsen A, Sinha R, Larsson E, Cerami E, Sander C, Schultz N. Integrative analysis of complex cancer genomics and clinical profiles using the cBioPortal. Science signaling. 2013; 6(269):1.

Guruharsha KG, Kankel MW, Artavanis-Tsakonas S. The Notch signalling system: recent insights into the complexity of a conserved pathway. Nature reviews Genetics. 2012; 13(9):654–666.

Guseh JS, Bores SA, Stanger BZ, Zhou Q, Anderson WJ, Melton DA, Rajagopal J. Notch signaling promotes airway mucous metaplasia and inhibits alveolar development. Development. 2009; 136(10):1751–1759. [PubMed: 19369400]

Haruki N, Kawaguchi KS, Eichenberger S, Massion PP, Olson S, Gonzalez A, Carbone DP, Dang TP. Dominant-negative Notch3 receptor inhibits mitogen-activated protein kinase pathway and the growth of human lung cancers. Cancer Res. 2005; 65(9):3555–3561. [PubMed: 15867348]

Ito T, Udaka N, Yazawa T, Okudela K, Hayashi H, Sudo T, Guillemot F, Kageyama R, Kitamura H. Basic helix-loop-helix transcription factors regulate the neuroendocrine differentiation of fetal mouse pulmonary epithelium. Development. 2000; 127(18):3913–3921. [PubMed: 10952889]

Jafar-Nejad H, Leonardi J, Fernandez-Valdivia R. Role of glycans and glycosyltransferases in the regulation of Notch signaling. Glycobiology. 2010; 20(8):931–949. [PubMed: 20368670]

Johnson L, Mercer K, Greenbaum D, Bronson RT, Crowley D, Tuveson DA, Jacks T. Somatic activation of the K-ras oncogene causes early onset lung cancer in mice. Nature. 2001; 410(6832): 1111–1116. [PubMed: 11323676]

Konishi J, Yi F, Chen X, Vo H, Carbone DP, Dang TP. Notch3 cooperates with the EGFR pathway to modulate apoptosis through the induction of bim. Oncogene. 2010; 29(4):589–596. [PubMed: 19881544]

Kopan R, Ilagan MX. The canonical Notch signaling pathway: unfolding the activation mechanism. Cell. 2009; 137(2):216–233. [PubMed: 19379690]

Krop I, Demuth T, Guthrie T, Wen PY, Mason WP, Chinnaiyan P, Butowski N, Groves MD, Kesari S, Freedman SJ, Blackman S, Watters J, Loboda A, Podtelezhnikov A, Lunceford J, Chen C, Giannotti M, Hing J, Beckman R, Lorusso P. Phase I pharmacologic and pharmacodynamic study of the gamma secretase (Notch) inhibitor MK-0752 in adult patients with advanced solid tumors. J Clin Oncol. 2012; 30(19):2307–2313. [PubMed: 22547604]

Kuramoto T, Goto H, Mitsuhashi A, Tabata S, Ogawa H, Uehara H, Saijo A, Kakiuchi S, Maekawa Y, Yasutomo K, Hanibuchi M, Akiyama S, Sone S, Nishioka Y. Dll4-Fc, an inhibitor of Dll4-notch signaling, suppresses liver metastasis of small cell lung cancer cells through the downregulation of the NF-kappaB activity. Molecular cancer therapeutics. 2012; 11(12):2578–2587. [PubMed: 22989420]

Leonardi J, Fernandez-Valdivia R, Li YD, Simcox AA, Jafar-Nejad H. Multiple O-glucosylation sites on Notch function as a buffer against temperature-dependent loss of signaling. Development. 2011; 138(16):3569–3578. [PubMed: 21771811]

Licciulli S, Avila JL, Hanlon L, Troutman S, Cesaroni M, Kota S, Keith B, Simon MC, Pure E, Radtke F, Capobianco AJ, Kissil JL. Notch1 is required for Kras-induced lung adenocarcinoma and controls tumor cell survival via p53. Cancer Res. 2013; 73(19):5974–5984. [PubMed: 23943799]

Lin L, Mernaugh R, Yi F, Blum D, Carbone DP, Dang TP. Targeting specific regions of the Notch3 ligand-binding domain induces apoptosis and inhibits tumor growth in lung cancer. Cancer Res. 2010; 70(2):632–638. [PubMed: 20068176]

Lleo A. Activity of gamma-secretase on substrates other than APP. Curr Top Med Chem. 2008; 8(1):9–16. [PubMed: 18220928]

Luo SY, Lam DC. Oncogenic driver mutations in lung cancer. Translational respiratory medicine. 2013; 1(1):6. [PubMed: 27234388]

Mainardi S, Mijimolle N, Francoz S, Vicente-Duenas C, Sanchez-Garcia I, Barbacid M. Identification of cancer initiating cells in K-Ras driven lung adenocarcinoma. Proc Natl Acad Sci U S A. 2014; 111(1):255–260. [PubMed: 24367082]

Maraver A, Fernandez-Marcos PJ, Herranz D, Canamero M, Munoz-Martin M, Gomez-Lopez G, Mulero F, Megias D, Sanchez-Carbayo M, Shen J, Sanchez-Cespedes M, Palomero T, Ferrando A, Serrano M. Therapeutic effect of gamma-secretase inhibition in KrasG12V-driven non-small cell lung carcinoma by derepression of DUSP1 and inhibition of ERK. Cancer Cell. 2012; 22(2):222–234. [PubMed: 22897852]

Moloney DJ, Shair LH, Lu FM, Xia J, Locke R, Matta KL, Haltiwanger RS. Mammalian Notch1 is modified with two unusual forms of O-linked glycosylation found on epidermal growth factor-like modules. J Biol Chem. 2000; 275(13):9604–9611. [PubMed: 10734111]

Morimoto M, Liu Z, Cheng HT, Winters N, Bader D, Kopan R. Canonical Notch signaling in the developing lung is required for determination of arterial smooth muscle cells and selection of Clara versus ciliated cell fate. Journal of cell science. 2010; 123(Pt 2):213–224. [PubMed: 20048339]

Morimoto M, Nishinakamura R, Saga Y, Kopan R. Different assemblies of Notch receptors coordinate the distribution of the major bronchial Clara, ciliated and neuroendocrine cells. Development. 2012; 139(23):4365–4373. [PubMed: 23132245]

Ntziachristos P, Lim JS, Sage J, Aifantis I. From fly wings to targeted cancer therapies: a centennial for notch signaling. Cancer Cell. 2014; 25(3):318–334. [PubMed: 24651013]

Osanyingbemi-Obidi J, Dobromilskaya I, Illei PB, Hann CL, Rudin CM. Notch signaling contributes to lung cancer clonogenic capacity in vitro but may be circumvented in tumorigenesis in vivo. Molecular cancer research : MCR. 2011; 9(12):1746–1754. [PubMed: 21994468]

Petersen I, Bujard M, Petersen S, Wolf G, Goeze A, Schwendel A, Langreck H, Gellert K, Reichel M, Just K, du Manoir S, Cremer T, Dietel M, Ried T. Patterns of chromosomal imbalances in

adenocarcinoma and squamous cell carcinoma of the lung. Cancer Res. 1997; 57(12):2331–2335. [PubMed: 9192802]

Purow B. Notch inhibition as a promising new approach to cancer therapy. Advances in experimental medicine and biology. 2012; 727:305–319. [PubMed: 22399357]

Regan JL, Sourisseau T, Soady K, Kendrick H, McCarthy A, Tang C, Brennan K, Linardopoulos S, White DE, Smalley MJ. Aurora A kinase regulates mammary epithelial cell fate by determining mitotic spindle orientation in a Notch-dependent manner. Cell reports. 2013; 4(1):110–123. [PubMed: 23810554]

Richer AL, Friel JM, Carson VM, Inge LJ, Whitsett TG. Genomic profiling toward precision medicine in non-small cell lung cancer: getting beyond EGFR. Pharmacogenomics and personalized medicine. 2015; 8:63–79. [PubMed: 25897257]

Schott AF, Landis MD, Dontu G, Griffith KA, Layman RM, Krop I, Paskett LA, Wong H, Dobrolecki LE, Lewis MT, Froehlich AM, Paranilam J, Hayes DF, Wicha MS, Chang JC. Preclinical and clinical studies of gamma secretase inhibitors with docetaxel on human breast tumors. Clin Cancer Res. 2013; 19(6):1512–1524. [PubMed: 23340294]

Schwaederle M, Elkin SK, Tomson BN, Carter JL, Kurzrock R. Squamousness: Next-generation sequencing reveals shared molecular features across squamous tumor types. Cell cycle. 2015; 14(14):2355–2361. [PubMed: 26030731]

Sutherland KD, Song JY, Kwon MC, Proost N, Zevenhoven J, Berns A. Multiple cells-of-origin of mutant K-Ras-induced mouse lung adenocarcinoma. Proc Natl Acad Sci U S A. 2014; 111(13): 4952–4957. [PubMed: 24586047]

Taichman DB, Loomes KM, Schachtner SK, Guttentag S, Vu C, Williams P, Oakey RJ, Baldwin HS. Notch1 and Jagged1 expression by the developing pulmonary vasculature. Developmental dynamics : an official publication of the American Association of Anatomists. 2002; 225(2):166–175. [PubMed: 12242716]

Takeuchi H, Fernandez-Valdivia RC, Caswell DS, Nita-Lazar A, Rana NA, Garner TP, Weldeghiorghis TK, Macnaughtan MA, Jafar-Nejad H, Haltiwanger RS. Rumi functions as both a protein O-glucosyltransferase and a protein O-xylosyltransferase. Proc Natl Acad Sci U S A. 2011; 108(40): 16600–16605. [PubMed: 21949356]

Thompson JC, Yee SS, Troxel AB, Savitch SL, Fan R, Balli D, Lieberman DB, Morrissette JD, Evans TL, Bauml J, Aggarwal C, Kosteva JA, Alley E, Ciunci C, Cohen RB, Bagley S, Stonehouse-Lee S, Sherry VE, Gilbert E, Langer C, Vachani A, Carpenter EL. Detection of therapeutically targetable driver and resistance mutations in lung cancer patients by next generation sequencing of cell-free circulating tumor DNA. Clin Cancer Res. 2016

Tien AC, Rajan A, Bellen HJ. A Notch updated. J Cell Biol. 2009; 184(5):621–629. [PubMed: 19255248]

Tolcher AW, Messersmith WA, Mikulski SM, Papadopoulos KP, Kwak EL, Gibbon DG, Patnaik A, Falchook GS, Dasari A, Shapiro GI, Boylan JF, Xu ZX, Wang K, Koehler A, Song J, Middleton SA, Deutsch J, Demario M, Kurzrock R, Wheler JJ. Phase I study of RO4929097, a gamma secretase inhibitor of Notch signaling, in patients with refractory metastatic or locally advanced solid tumors. J Clin Oncol. 2012; 30(19):2348–2353. [PubMed: 22529266]

Tsao PN, Matsuoka C, Wei SC, Sato A, Sato S, Hasegawa K, Chen HK, Ling TY, Mori M, Cardoso WV, Morimoto M. Epithelial Notch signaling regulates lung alveolar morphogenesis and airway epithelial integrity. Proc Natl Acad Sci U S A. 2016; 113(29):8242–8247. [PubMed: 27364009]

Tsao PN, Vasconcelos M, Izvolsky KI, Qian J, Lu J, Cardoso WV. Notch signaling controls the balance of ciliated and secretory cell fates in developing airways. Development. 2009; 136(13):2297–2307. [PubMed: 19502490]

Unni AM, Lockwood WW, Zejnullahu K, Lee-Lin SQ, Varmus H. Evidence that synthetic lethality underlies the mutual exclusivity of oncogenic KRAS and EGFR mutations in lung adenocarcinoma. eLife. 2015; 4:e06907. [PubMed: 26047463]

Wang Z, Li Y, Banerjee S, Sarkar FH. Emerging role of Notch in stem cells and cancer. Cancer letters. 2009; 279(1):8–12. [PubMed: 19022563]

Westhoff B, Colaluca IN, D'Ario G, Donzelli M, Tosoni D, Volorio S, Pelosi G, Spaggiari L, Mazzarol G, Viale G, Pece S, Di Fiore PP. Alterations of the Notch pathway in lung cancer. Proc Natl Acad Sci U S A. 2009; 106(52):22293–22298. [PubMed: 20007775]

Xu K, Nieuwenhuis E, Cohen BL, Wang W, Canty AJ, Danska JS, Coultas L, Rossant J, Wu MY, Piscione TD, Nagy A, Gossler A, Hicks GG, Hui CC, Henkelman RM, Yu LX, Sled JG, Gridley T, Egan SE. Lunatic Fringe-mediated Notch signaling is required for lung alveogenesis. American journal of physiology Lung cellular and molecular physiology. 2010; 298(1):L45–56. [PubMed: 19897741]

Xu X, Huang L, Futtner C, Schwab B, Rampersad RR, Lu Y, Sporn TA, Hogan BL, Onaitis MW. The cell of origin and subtype of K-Ras-induced lung tumors are modified by Notch and Sox2. Genes Dev. 2014; 28(17):1929–1939. [PubMed: 25184679]

Xu X, Rock JR, Lu Y, Futtner C, Schwab B, Guinney J, Hogan BL, Onaitis MW. Evidence for type II cells as cells of origin of K-Ras-induced distal lung adenocarcinoma. Proc Natl Acad Sci U S A. 2012; 109(13):4910–4915. [PubMed: 22411819]

Xu Y, Wang Y, Liu H, Kang X, Li W, Wei Q. Genetic variants of genes in the Notch signaling pathway predict overall survival of non-small cell lung cancer patients in the PLCO study. Oncotarget. 2016

Yang Y, Ahn YH, Gibbons DL, Zang Y, Lin W, Thilaganathan N, Alvarez CA, Moreira DC, Creighton CJ, Gregory PA, Goodall GJ, Kurie JM. The Notch ligand Jagged2 promotes lung adenocarcinoma metastasis through a miR-200-dependent pathway in mice. The Journal of clinical investigation. 2011; 121(4):1373–1385. [PubMed: 21403400]

Yuan X, Wu H, Xu H, Han N, Chu Q, Yu S, Chen Y, Wu K. Meta-analysis reveals the correlation of Notch signaling with non-small cell lung cancer progression and prognosis. Scientific reports. 2015; 5:10338. [PubMed: 25996086]

Zhang S, Loch AJ, Radtke F, Egan SE, Xu K. Jagged1 is the major regulator of Notch-dependent cell fate in proximal airways. Developmental dynamics : an official publication of the American Association of Anatomists. 2013; 242(6):678–686. [PubMed: 23526493]

Zheng Y, de la Cruz CC, Sayles LC, Alleyne-Chin C, Vaka D, Knaak TD, Bigos M, Xu Y, Hoang CD, Shrager JB, Fehling HJ, French D, Forrest W, Jiang Z, Carano RA, Barck KH, Jackson EL, Sweet-Cordero EA. A rare population of CD24(+)ITGB4(+)Notch(hi) cells drives tumor propagation in NSCLC and requires Notch3 for self-renewal. Cancer Cell. 2013; 24(1):59–74. [PubMed: 23845442]

Zhou M, Jin WY, Fan ZW, Han RC. Analysis of the expression of the Notch3 receptor protein in adult lung cancer. Oncology letters. 2013; 5(2):499–504. [PubMed: 23420695]

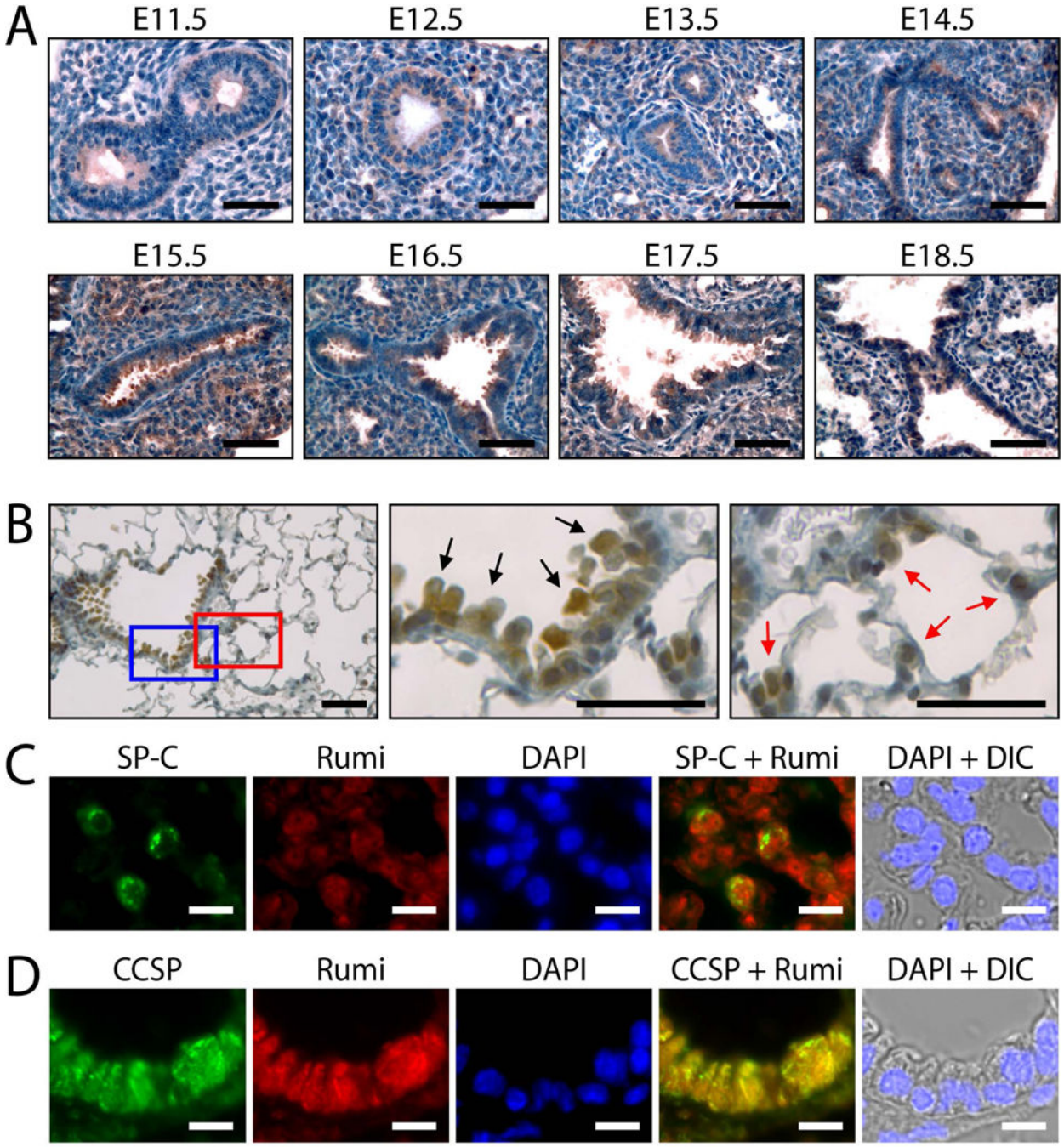

Figure 1. Rumi is expressed in both alveolar type II cells and bronchiolar Club cells, and its expression is dynamically controlled during lung morphogenesis

(A) Rumi immunohistochemistry stainings in distinct embryonic and fetal lung developmental stages showing dynamic expression of Rumi (brown staining) in the lung epithelium. Rumi expression becomes noticeable during the late embryonic stage of lung development (E11.5) and is mostly restricted to the endoderm-derived epithelium. Rumi levels gradually increase during the pseudoglandular stage (E12.5 – E15.5) in both the proximal and distal epithelium, and reach high levels of expression at E15.5 developmental

stage, a key developmental window marked by pronounced branching morphogenesis. Rumi is expressed in the proximal and distal lung epithelium during the canalicular (E15.5 – E17.5) and saccular (E18.5) stages, and its expression becomes more pronounced in the proximal epithelium. Scale bar, 50 μm. **(B)** Rumi immunohistochemical staining showing Rumi expression (brown color) in the bronchiolar (black arrows in middle image) and alveolar (red arrows in right image) epithelia. The blue and red rectangles in the low-magnification image (left) correspond, respectively, to the regions displayed at high magnification in the middle and right images. Scale bars, 50 μm. **(C)** Dual immunofluorescence staining for Rumi and surfactant protein C (SP-C) demonstrating that Rumi is expressed in type II pneumocytes (yellow signal in overlaid co-localization image). DIC, Differential Interference Contrast. Scale bar, 10 μm. **(D)** Rumi and Club cell secretory protein (CCSP) dual immunofluorescence staining showing that Rumi is expressed in bronchiolar Club cells (yellow signal in the overlaid co-localization image). Scale bar, 10 μm.

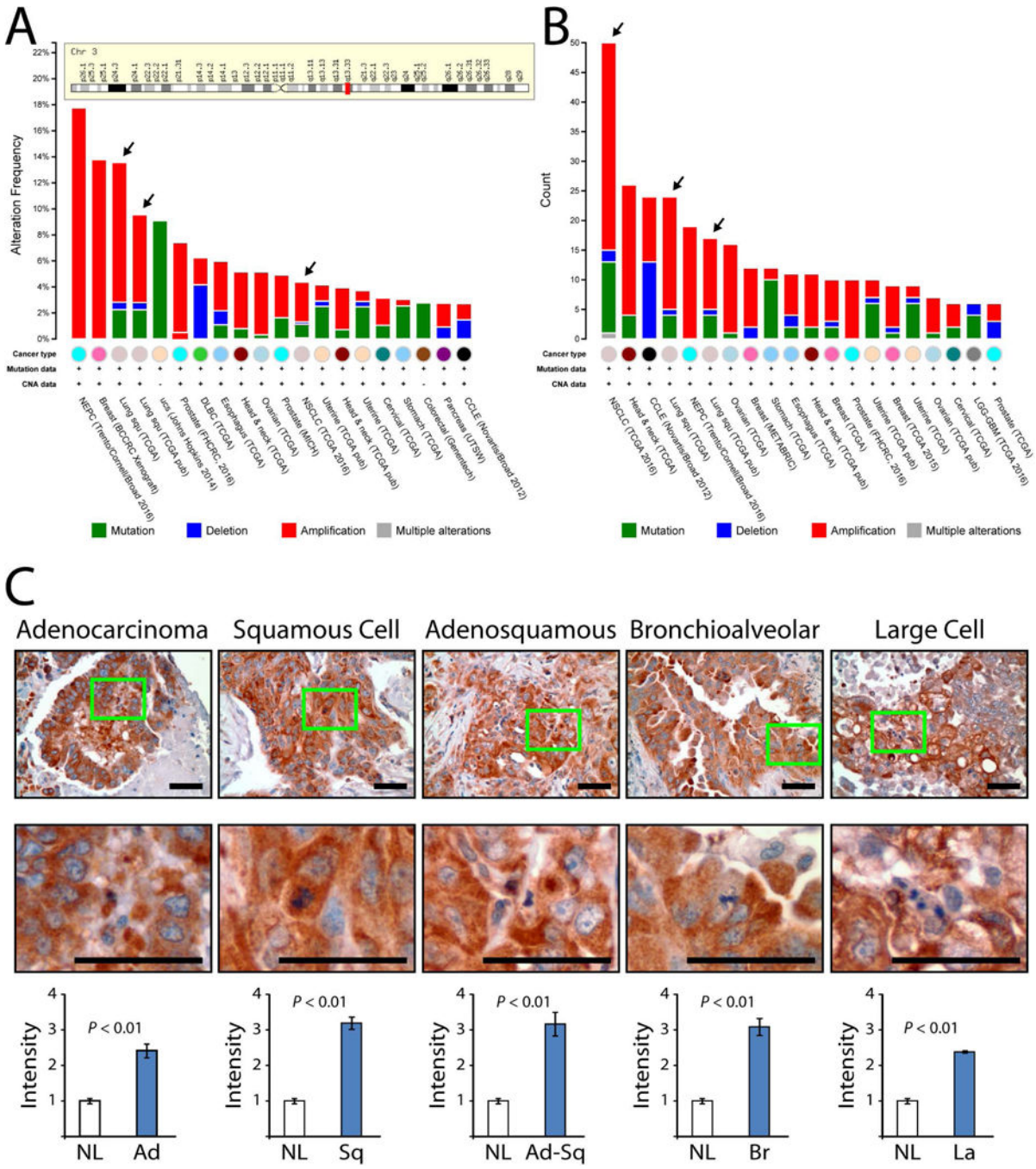

Figure 2. *RUMI* is amplified and highly expressed in Non-Small Cell Lung Cancer

(A) Cross-cancer genomic alteration graph for *RUMI* from 164 independent studies indicating strong correlation of *RUMI* amplification frequency with lung squamous cell carcinoma (arrows in bars 3 and 4) and, in general, NSCLC (arrow in bar 12). Only the top-20 studies showing the highest numbers of *RUMI* alterations are displayed. The inset chromosome 3 diagram shows the location of *RUMI* (red bar) in 3q13.33. **(B)** Cross-cancer genomic alteration summary for *RUMI* from 164 independent studies indicating total number of cases per genetic alteration. Note that *RUMI* amplification is observed in greater

numbers in NSCLC (arrow in bar 1) and, in particular, in lung squamous cell carcinoma (arrows in bars 4 and 6). Genetic alterations mining include mutation, deletion, amplification or multiple alterations. Data was obtained from the cBioportal for cancer genomics (http://www.cbioportal.org/public-portal/, Memorial Sloan-Kettering Cancer Center, NY, NY) and GeneCards (http://www.genecards.org/, Weizmann Institute of Science, Rehovot, Israel). **(C)** RUMI immunohistochemistry experiments showing high levels of RUMI expression in distinct sub-types of Non-Small Cell Lung Cancer (NSCLC) tumors. A polyclonal antibody against RUMI (Basmanav et al., 2014) was used to perform immunodetection of RUMI in three independent lung cancer tumor microarrays (US Biomax) containing cores of the indicated NSCLC subtypes. The green rectangles in the top microphotographs correspond to the regions shown at high magnification in the microphotographs below. Note the intense RUMI signal in tumor cells compared to adjacent stromal regions. Also, note the presence of actively dividing cells with partially-condensed nuclei in the regions marked by strong RUMI immunoreactivity. The graphs in the bottom show RUMI immunostaining intensity score averages ± SEM for the corresponding NSCLC tumor subtypes against normal lung. Obtained intensity scores were: lung adenocarcinoma, 2.4 fold; squamous cell carcinoma, 3.2 fold; adenosquamous cell carcinoma, 3.2 fold; bronchioalveolar carcinoma, 3.1 fold; large cell carcinoma, 2.4 fold. The comparative score averages in the graphs were normalized to allow visualization of RUMI expression level fold change in distinct NSCLC tumors compared to normal lung tissue. NL, Normal Lung; Ad, Adenocarcinoma; Sq, Squamous Cell Carcinoma; Ad-Sq, Adenosquamous Cell Carcinoma; Br, Bronchioalveolar Carcinoma; La, Large Cell Carcinoma. Scale bars, 50 μm.

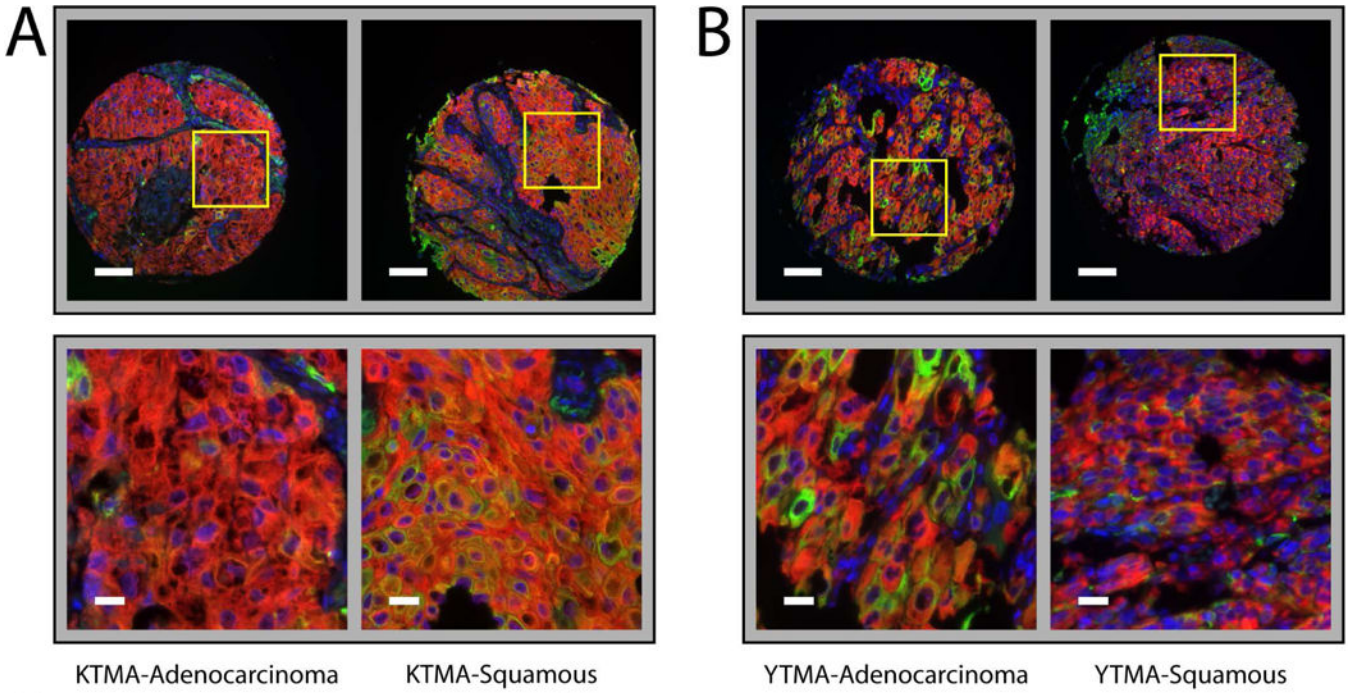

C

Multivariable Cox model for training data KTMA and validation data YTMA

	KTMA		YTMA	
	HR (95% CI)	P value	HR (95% CI)	P value
Group				
Low	Ref.		Ref.	
High	1.81 (1.08, 3.01)	0.023	2.89 (1.17, 7.16)	0.022
Sex				
Female	Ref.		Ref.	
Male	1.34 (0.85, 2.11)	0.208	1.22 (0.71, 2.09)	0.48
Stage				
I	Ref.		Ref.	
>I	0.87 (0.37, 2.05)	0.758	2.51 (1.48, 4.27)	0.001
Histology				
Adeno	Ref.		Ref.	
Squamous	0.88 (0.56, 1.37)	0.56	0.93 (0.52, 1.66)	0.811
Age	1.04 (1.01, 1.07)	0.006	0.99 (0.96, 1.02)	0.387

D

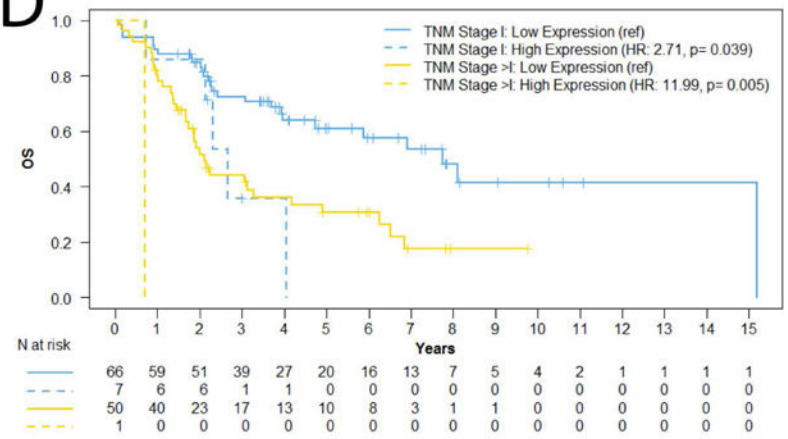

Figure 3. RUMI is a strong negative prognostic factor in NSCLC

(A) Representative images of Automated Quantitative Analysis (AQUA) for RUMI expression (red fluorescence) in adenocarcinoma (N=97) and squamous cell carcinoma (N=131) cores performed in Karmanos Cancer Institute's NSCLC Tissue Microarrays (KTMA). A pan-cytokeratin antibody (DAKO AE1/AE3, green fluorescence) was used for immunotyping. Nuclei were stained with DAPI. The regions marked by yellow squares are shown at high magnification in the second row microphotographs. Scale bars are 100 μm for top images and 20 μm for bottom images. **(B)** Representative images of AQUA analyses for validation of RUMI expression in adenocarcinoma (N=118) and squamous cell carcinoma (N=37) cores performed in Yale Cancer Center's NSCLC Tissue Microarrays (YTMA). A pan-cytokeratin antibody (DAKO AE1/AE3, green fluorescence) was used for immunotyping. Nuclei were stained with DAPI. Staining conditions and AQUA imaging and analysis parameters were identical to the ones used for KTMA slides. The regions marked

by yellow squares are shown at high magnification in the second row microphotographs. Scale bars are 100 μm for top images and 20 μm for bottom images. **(C)** Table displaying the results of Multivariable Cox model analysis for KTMA training data and YTMA validation data. Note the strong association between high levels of RUMI expression and increased hazard ratio (HR) in both KTMA (P=0.023) and YTMA (P=0.022). CI, Confidence Interval. **(D)** Kaplan-Meier (KM) plot of Overall Survival (OS) on validation data YTMA stratified on stage, using the optimal cutoff of high/low RUMI expression identified from training data KTMA. Median OS for Stage I and low expression was 7.757 years 95%CI (4.74 ~NA); Median OS for Stage I and high expression was 2.66 years 95%CI (2.14 ~NA); Median OS for Stage >I and low expression was 2.11 years 95%CI (1.75 ~ 4.91); Median OS for Stage >I and high expression was 0.711 years 95%CI (NA~NA). Patients with high RUMI expression had worse prognosis.

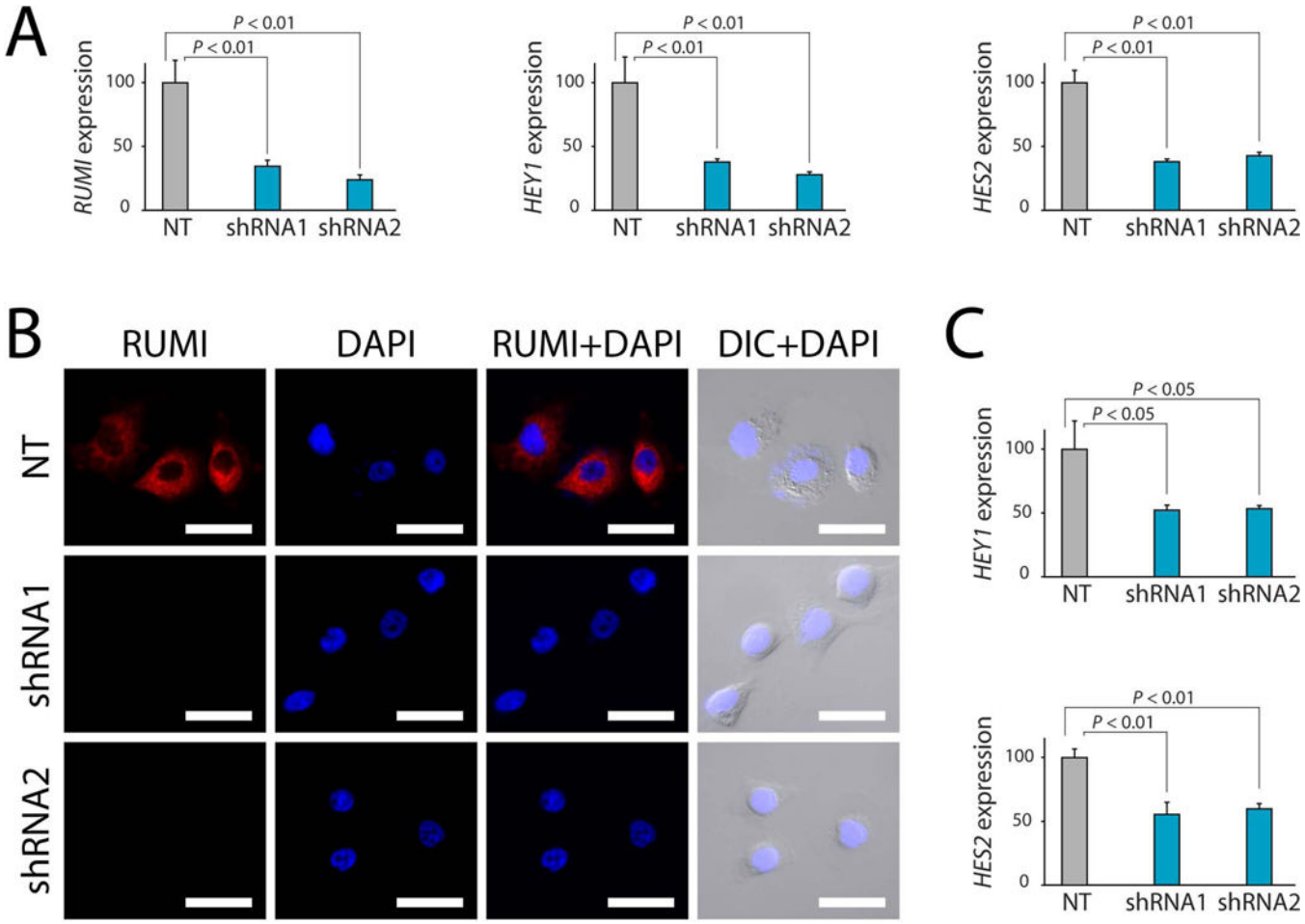

Figure 4. RUMI silencing inhibits Notch signaling in NSCLC cells

(A) RNAi-mediated *RUMI* knockdown in A549 cells demonstrating effective *RUMI* silencing and Notch signaling inhibition by two independent and non-overlapping *RUMI*-targeted shRNAs. *RUMI* knockdown effectively silences *RUMI* expression and inhibits Notch signaling activity, as evidenced, respectively, by the significant decrease in mRNA levels of *RUMI* and Notch downstream targets *HEY1* and *HES2*. **(B)** RNAi-mediated *RUMI* knockdown and immunofluorescence experiments demonstrating effective RUMI silencing in H23 cells. Note that these shRNA data also confirms specificity of the antibody used for human RUMI immunodetection. Scale bar, 30 μm. **(C)** shRNA-mediated *RUMI* knockdown effectively inhibits Notch signaling activation in H23 cells, as evidenced by the significant decrease in mRNA levels of Notch downstream effectors *HEY1* and *HES2*. RT-qPCR experiments were performed using Taqman assays for human *RUMI*, *HEY1* and *HES2* genes and the $2^{-\Delta\Delta Cq}$ method using 18S rRNA as reference. Data shown as mean ± SD.

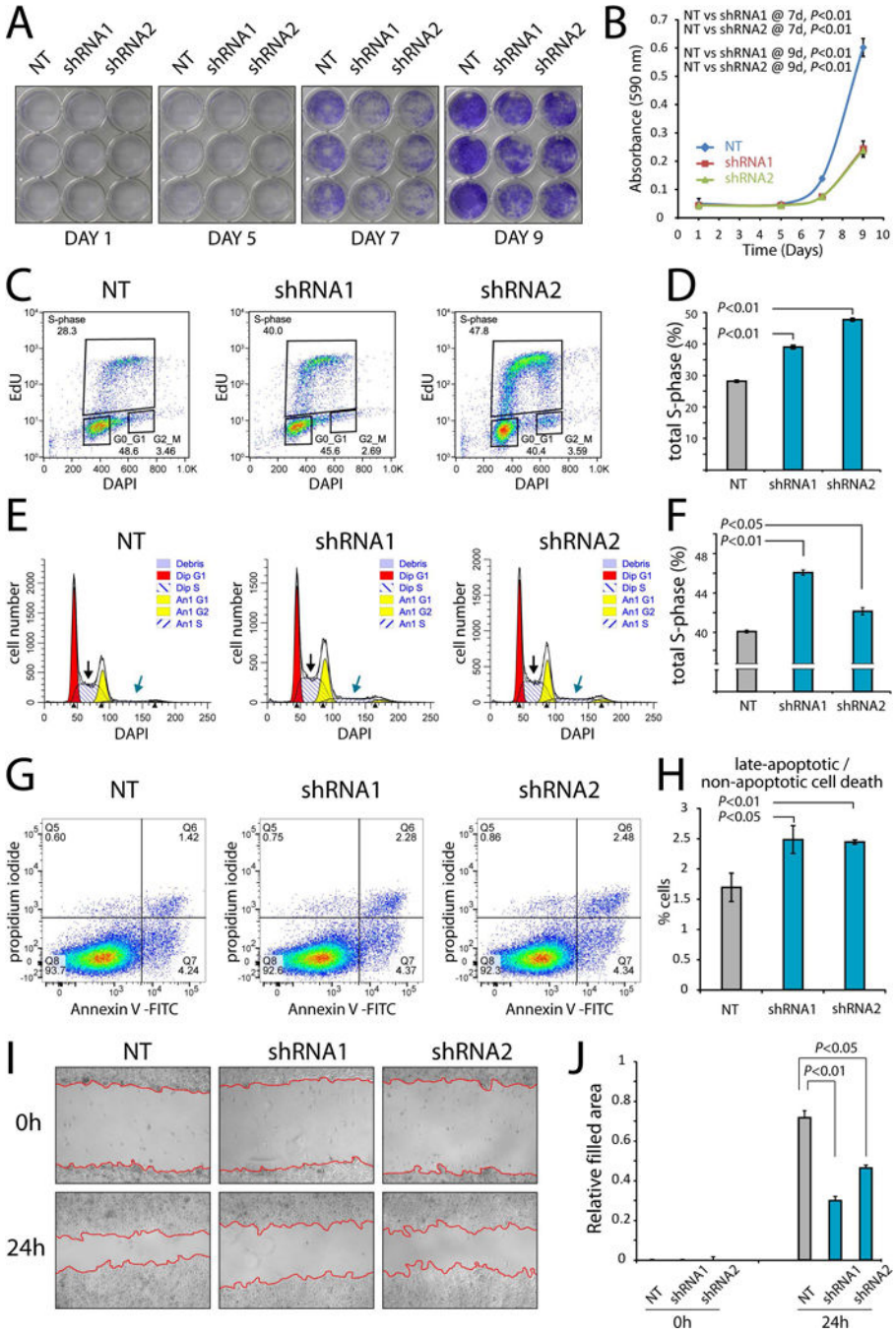

Figure 5. *RUMI* silencing inhibits cell proliferation, migration and survival in NSCLC cell lines

(A) *RUMI* knockdown and crystal violet cell proliferation experiments in A549 NSCLC cells demonstrating that *RUMI* silencing dramatically decreases cell proliferation. Two independent and non-overlapping shRNAs targeting human *RUMI* and three biological samples per knockdown assay were used. NT, non-target control. **(B)** Quantification and statistical analysis of crystal violet assays demonstrating that *RUMI* silencing causes a highly significant decrease ($P<0.01$, two-tail t-test, mean ± SD) in cell proliferation in A549 cells. **(C)** Cell cycle analysis (DAPI/EdU incorporation assay) experiments demonstrating

that RNAi-mediated *RUMI* knockdown causes a dramatic S-phase arrest in A549 NSCLC cells. **(D)** Quantification of total S-phase cell fraction in DAPI/EdU assays demonstrating that *RUMI* silencing causes a highly significant ($P<0.01$, two-tail t-test, mean ± SD) increase in the total S-phase fraction (measured by EdU incorporation) in A549 NSCLC cells. **(E)** High resolution DAPI and DNA ploidy cell cycle analysis (DAPI assay and ModFit modeling) demonstrating that *RUMI* silencing causes a marked S-phase arrest and increased genome instability in H23 NSCLC cells. Note that in comparison to Non-target control H23 cells, *RUMI*-silenced cells display not only S-phase arrest (compare the curves indicated by black arrows) during their cell cycle progression (algorithmically modeled as diploid cell cycle for comparative purposes, Dip S in graphs), but also display a further marked aneuploidy as evidenced by the striking appearing of single cells containing twice the amount of DNA (algorithmically modeled as aneuploid cell cycle for comparative purposes, An1 in graphs) and undergoing cell cycle progression (see curves corresponding to An1 G1, An1 G2 and An1 S in graphs). Notably, these further aneuploid cells also display a marked S-phase arrest (see regions indicated by light blue arrows between *RUMI*-silenced and control cells). **(F)** Quantification and statistical analysis of the flow cytometry experiments in control and *RUMI*-silenced H23 cells indicating that *RUMI* knockdown causes a pronounced increase in the total S-phase fraction (DAPI/ModFit modeling). Note that this marked increase is highly statistically significant for shRNA1 ($P<0.01$, two-tail t-test, mean ± SD) and statistically significant for shRNA2 ($P<0.05$, two-tail t-test, mean ± SD). Importantly, the S-phase arrest displayed by H23 *RUMI*-silenced cells is statistically significant not only when evaluated as total S-phase, but also when quantified separately for either N-ploid cells (algorithmically modeled as diploid for comparative purposes, Dip in graphs) and further aneuploid cells (modeled and aneuploid An1) (Fig. S4C, D). **(G)** Representative flow cytometry plots of Annexin-V/propidium iodide (PI) assays in control and *RUMI*-silenced A549 cells. Note that *RUMI* knockdown causes a pronounced increase in late-apoptotic/non-apoptotic cell death (Annexin-V^+PI^+, Q6 quadrant) without significantly affecting the fraction of cells undergoing early apoptosis (Annexin-V^+PI^-, Q7 quadrant). **(H)** Quantification and statistical analysis of Annexin-V/PI flow cytometry experiments indicating that shRNA-mediated *RUMI* silencing causes a marked increase in the fraction of cells undergoing late-apoptotic/non-apoptotic cell death. Note that this pronounced increase is statistically significant in cells stably transfected with shRNA1 ($P<0.05$, two-tail t-test, mean ± SEM) and highly statistically significant in cells stably transfected with shRNA2 ($P<0.01$, two-tail t-test, mean ± SEM). **(I)** Scratch assay experiments in control and *RUMI*-silenced H23 cells demonstrating that *RUMI* knockdown causes a marked decrease in cell migration. **(J)** Quantification and statistical analysis of the filled scratch area demonstrating that *RUMI* silencing markedly decreases cell migration in H23 NSCLC cells. Note that this marked decrease is statistically significant for cells expressing shRNA2 ($P<0.05$, two-tail t-test, mean ± SEM) and highly statistically significant for cells expressing shRNA1 ($P<0.01$, two-tail t-test, mean ± SEM).